How to cite: *Angew. Chem. Int. Ed.* **2024**, *63*, e202405120
doi.org/10.1002/anie.202405120

Enzyme Mechanisms

Coupling CO_2 Reduction and Acetyl-CoA Formation: The Role of a CO Capturing Tunnel in Enzymatic Catalysis

*Jakob Ruickoldt, Jae-Hun Jeoung, Maik Alexander Rudolph, Frank Lennartz, Julian Kreibich, Reinhard Schomäcker, and Holger Dobbek**

Abstract: The bifunctional CO-dehydrogenase/acetyl-CoA synthase (CODH/ACS) complex couples the reduction of CO_2 to the condensation of CO with a methyl moiety and CoA to acetyl-CoA. Catalysis occurs at two sites connected by a tunnel transporting the CO. In this study, we investigated how the bifunctional complex and its tunnel support catalysis using the CODH/ACS from *Carboxydothermus hydrogenoformans* as a model. Although CODH/ACS adapted to form a stable bifunctional complex with a secluded substrate tunnel, catalysis and CO transport is even more efficient when two monofunctional enzymes are coupled. Efficient CO channeling appears to be ensured by hydrophobic binding sites for CO, which act in a bucket-brigade fashion rather than as a simple tube. Tunnel remodeling showed that opening the tunnel increased activity but impaired directed transport of CO. Constricting the tunnel impaired activity and CO transport, suggesting that the tunnel evolved to sequester CO rather than to maximize turnover.

Introduction

The reductive acetyl-CoA pathway allows the simultaneous fixation of two molecules of CO_2 to acetate, generating ATP in the process.[1,2] It is one of the most energy-efficient biological carbon fixation pathways, making it a promising candidate for the production of renewable fuels. The CO-dehydrogenase/acetyl-CoA-synthase (CODH/ACS) complex catalyzes the final step of this pathway: the formation of acetyl-CoA from CO_2, reducing equivalents, a methyl-cation, and coenzyme A. Bacterial CODH/ACS complexes consist of a CODH-homodimer carrying two ACS subunits on each side.[3–6]

The synthesis of acetyl-CoA takes place in the enzyme complex in two partial reactions (reviewed by Can et al.[7]). First, CO_2 is reduced to CO at the C-cluster (a [$NiFe_4(OH)$-(μ_3-$S)_4$] cluster) of the CODH subunit. The generated CO then travels through a 70 Å long tunnel to the A-cluster in the ACS subunit. The A-Cluster is a Ni,Ni-[4Fe4S] cluster which catalyzes the condensation of CO, a methyl-cation (donated by the corrinoid-Fe–S-protein (CoFeSP) and CoA.[4,8,9] A scheme of the proposed catalytic cycle at the A-cluster can be found in Figure S1.

The ACS subunit can adopt at least two conformations that affect the CO tunnel: open and closed. In the open conformation the A-cluster is solvent-exposed and the tunnel between the C-cluster and the A-cluster is closed. In the closed conformation the A-cluster is buried and the tunnel is continuous.[3,4] So far, it is not known what triggers the switch between these conformations.

The presence of the tunnel in the CODH/ACS complex was proposed even before structure information was available.[10,11] This was based on the fact that, despite the very high affinity of hemoglobin for CO, hemoglobin did not strongly inhibit the channeling of CO into acetyl-CoA. The presence of a hydrophobic tunnel was later confirmed by the first crystal structures.[3,4,12]

The role of the tunnel in catalysis has been investigated in several studies using the CODH/ACS complex from *Moorella thermoacetica*.[13–15] Constrictions in the tunnels connecting the two C-clusters in the CODH-homodimer to each other and to solvent decreased CO oxidation activity and acetyl-CoA synthesis from CO_2.[14] However, constrictions in the tunnel connecting the C-cluster and the A-cluster did not severely affect the CO oxidation activity but almost eliminated the production of acetyl-CoA from CO_2.[13] In addition, the activity in the condensation reaction was no longer inhibited by CO in the narrow-tunnel variants but was significantly lower than the wild-type activity. This led to the dual-pathway hypothesis,[14] which states that the CO coming through the tunnel reacts in the correct step of catalysis while the CO approaching the A-cluster from the

[*] Dr. J. Ruickoldt, Dr. J.-H. Jeoung, Dr. J. Kreibich, Prof. Dr. H. Dobbek
Humboldt-Universität zu Berlin
Institut für Biologie
Unter den Linden 6, 10099 Berlin, Germany
E-mail: holger.dobbek@hu-berlin.de
M. A. Rudolph, Prof. Dr. R. Schomäcker
Technische Universität Berlin
Institut für Chemie - Technische Chemie
Straße des 17. Juni 124, 10623 Berlin, Germany
Dr. F. Lennartz
Helmholtz-Zentrum Berlin
Macromolecular Crystallography
Albert-Einstein-Straße 15, 12489 Berlin, Germany

solvent inhibits catalysis by binding non-productively in an earlier catalytic step. In what ways catalysis benefits from carrying out the coupled reaction within a stable bifunctional protein complex harboring a long gas tunnel in contrast to two monofunctional enzymes, is not known.

To clarify this, we took advantage of the unique properties of the ACS from *C. hydrogenoformans* to act as a single, monofunctional enzyme or to be part of a stable, bifunctional complex with CODH-III.[9] We inferred the phylogeny of the CODHs and show how the structure has adapted as complex-forming CODHs evolved. We then assessed whether the stable CODH/ACS complex is catalytically superior to the monofunctional enzymes, and finally analyzed the role of the tunnel in the bifunctional complex by site-directed mutagenesis.

Results and Discussion

Phylogeny of the CODH Subunit

We used the genomic proximity of the genes encoding CODH and ACS as a guide to discriminate between mono- and bifunctional CODHs (Figure S2). This approach correctly identified the sequences of currently known bifunctional CODH/ACS complexes, including the *M. thermoacetica* CODH, *C. hydrogenoformans* CODH-III, and *C. autoethanogenum* CODH. Conversely, none of the known monofunctional CODHs were predicted to be bifunctional or encoded by a gene proximal to a gene encoding an ACS. The inferred phylogeny indicates that the CODH/ACS complexes of *M. thermoacetica* and *C. hydrogenoformans* (bifunctional type I), on the one hand, and the complex of *C. autoethanogenum* (bifunctional type II), on the other hand, evolved independently (Figure S2). This is consistent with the various structural differences between the two complexes, which differ in their binding interfaces, structural motifs to stabilize the complex, and the tunnels within CODH and connecting the active sites of CODH and ACS. Here, we focus on the structural evolution of the *Moorella* / *Carboxydothermus* type I bifunctional CODHs. Whereas monofunctional CODHs have gas tunnels that span the entire dimer and connect the active site cluster to the molecular surface, bifunctional type I CODHs have blocked channels to the surface and CO_2 diffusion into the active site requires structural dynamics that control substrate access to the C-cluster.[16] We followed the evolution of the residues lining the tunnel of monofunctional CODHs and found that the smaller side chains near the tunnel exit found in monofunctional CODHs, such as CODH-II and the CODH from *Rhodospirillum rubrum*, are present in the last common ancestor of monofunctional CODHs and bifunctional type I CODHs (AncB; see Figure 1, Figure S3), but that these residues were replaced by bulkier side chains, predominantly phenylalanines in the transition to the last common ancestor of bifunctional CODHs (AncC; Figure 1, Figure S3). These bulky side chains block the tunnel exit, closing the connection between the C-cluster and the surface.

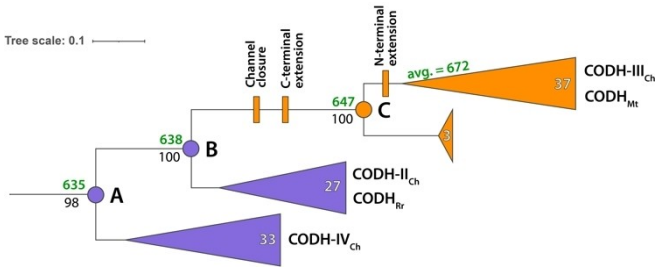

Figure 1. Phylogeny of type-I bifunctional CODHs. A, B and C denote three ancestral states. Their sequence lengths are shown in green, black numbers near internal nodes are non-parametric bootstrap scores, showing that the proposed clades are well supported. CODH-II$_{Ch}$, CODH-IV$_{Ch}$ and CODH$_{Rr}$ are exemplary monofunctional CODHs, CODH-III$_{Ch}$ and CODH$_{Mt}$ bifunctional CODHs. Lower case Ch denotes *Carboxydothermus hydrogenoformans* CODHs, Rr stands for *Rhodospirillum rubrum* and Mt for *Moorella thermoacetica*. Numbers within the collapsed clades give the number of sequences in the clade. Change in color from violet to orange denotes the hypothetical switch from monofunctional to bifunctional CODHs with the character state changes shown above the branches. For the complete phylogeny, see Figure S2.

Ancestral sequence reconstruction points to a second hotspot of changes in the transition from mono- to bifunctional CODHs (AncB to AncC, Figure 1). In the structures of the CODH/ACS complex from *M. thermoacetica* and *C. hydrogenoformans*, the N- and C-terminal extensions of the CODH subunit interact closely with the ACS subunit, stabilizing the complex. These extensions began to evolve during the transition from the common ancestor of monofunctional CODHs (AncB) to the ancestors of bifunctional CODHs (AncC), with the C-terminal helix extending before the N-terminal loop extension (Figure 1). These structural elements are absent from the common ancestor of monofunctional and bifunctional CODHs (AncB), which is more similar in length to extant monofunctional CODHs (Figure S4).

What is the Advantage of a Bifunctional Complex?

We analyzed the transport of CO during catalysis using a competition experiment. Here, the synthesis of acetyl-CoA from CO_2 was followed in the presence of hemoglobin, which binds free CO with high affinity ($K_d = 84$ nM, Figure S5). For the CODH/ACS complex, the carboxy-hemoglobin complex (Hb-CO) formed only after the rate of acetyl-CoA synthesis ceased due to the consumption of methylcobinamide and CoA (Figure 2b). Thus, CO was channeled into acetyl-CoA as long as all substrates were present, as found before.[10,11] However, we wondered if a tight bifunctional complex is essential for efficient channeling of CO into acetyl-CoA. Therefore, we performed the same experiment with the monofunctional CODH-II and the isolated ACS subunit. Surprisingly, even with the monofunctional enzymes, Hb-CO formed only after acetyl-CoA synthesis had stopped (Figure 2d). Apparently, the A-cluster has a higher affinity towards CO than hemoglobin.

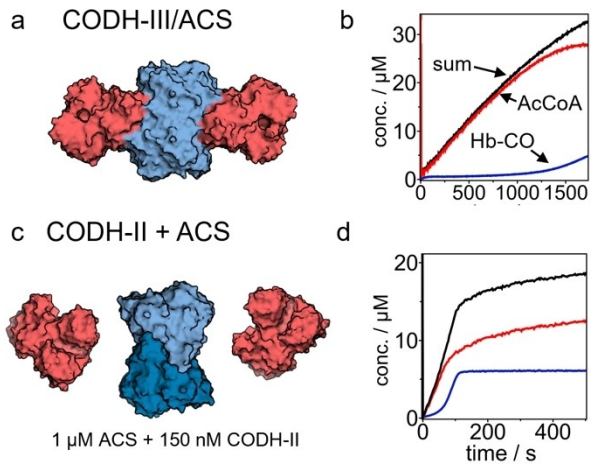

Figure 2. CO transport during catalysis for the CODH/ACS complex variants and the isolated ACS subunit coupled with CODH-II. The competition experiment was always carried out in 0.1 M Mops/NaOH pH 7.2 supplemented with 0.3 mg/L carbonic anhydrase, 7 µM Hb, 200 µM CoA, 50 µM methylcobinamide, 10 mM Ti(III)-EDTA, and 1.2 mM CO_2, if not otherwise stated. a) Structure of the CODH/ACS complex (PDB 7ZKJ). ACS red, CODH-III blue. b) Competition experiment traces for the CODH-III/ACS complex (0.22 µM). c) CODH-II (light and dark blue, PDB 4UDX) and the isolated ACS subunit (red, PDB 7ZKJ). d) Competition experiment traces for the coupled action of ACS (1 µM) and CODH-II (150 nM).

To test this, we performed ITC experiments (Figure S6). In the reduced state, the A-cluster has a K_d for CO of about 750 nM, which is not enough to outcompete hemoglobin. However, in the methylated state the K_d drops to 12 nM, probably due to the immediate insertion of the CO into the Ni–CH_3 bond.[17] This is about 8-times lower than the K_d of hemoglobin determined here (Figure S5). Still, even such a low affinity of the methylated A-cluster for CO is insufficient to explain the observed kinetics: due to the approximately 14-fold excess of hemoglobin over ACS in the assays (assuming a degree of maturation of 50 % for ACS), Hb-CO should still be able to compete with methylated ACS for CO binding.

Three hypotheses may explain this observation: First, CODH-II and ACS form a complex with a continuous gas tunnel, second, the binding of CO to the A-cluster is much faster than that to Hb, or third, there is a partition equilibrium for CO being in water or in the hydrophobic tunnel creating a pool of CO connected to the A-cluster but inaccessible to hemoglobin. The first hypothesis is unlikely, as size-exclusion co-injection experiments of ACS and CODH-II showed neither a peak corresponding to a stable complex nor a change of retention times or peak shapes indicative of transient complex formation (Figure S8).[18] Furthermore, CODH-II lacks the structural elements that have evolved in the bifunctional CODHs to stabilize a complex with ACS. While we cannot completely rule out the formation of weak transient CODH-II/ACS complexes, the majority of CODH-II molecules would be uncomplexed and dominate CO generation. At this point, we cannot distinguish between hypothesis 2 and 3 and will return to this question in the section "CO transport in the variants".

Remodeling the Intramolecular CO Tunnel

To understand why such a long and complex tunnel evolved in CODH/ACS, we used site-directed mutagenesis to investigate its role in catalysis. Two amino acid exchanges in the ACS subunit (A225L and A268M) were designed to restrict the tunnel between the C-cluster and the A-cluster, two others (F231A in CODH-III and F515A in ACS) were designed to open the tunnel system and finally, the combination of a restricting and an opening double exchange (A225L/F231A) was investigated. All variants were structurally and kinetically characterized.

We previously reported the structures of the wild-type complex and the F231A variant at resolutions of 2.04 Å (WT) and 2.07 Å (F231A).[6] In this study, we resolved the crystal structures of the remaining variants at resolutions of 2.60 Å (A225L), 2.62 Å (A268M), 2.22 Å (F515A), and 2.10 Å (A225L/F231A)(See Table S3 for statistics of the X-ray diffraction data and model refinement).

The overall structures of the tunnel variants and wild-type CODH/ACS are indistinguishable. The RMSD of Cα-atoms positions between the wild-type and variant structures were not greater than the estimated coordinate error (Table S1). With the exception of F515A, the environment at the mutation site was not perturbed (Figure S9). The F515A exchange resulted in a slight rearrangement of a loop, which in turn caused a movement of a neighboring arginine (Arg250; Figure S9b). However, this arginine is on the surface of the protein and its rearrangement does not cause any further changes in the tunnel. Indirect effects on the tunnel dynamics, such as changes of the conformational equilibrium between the open and closed conformation of ACS in solution, cannot be ruled out.

The tunnel system was analyzed computationally using CaverAnalyst 2.0[19] with a probe radius of 0.9 Å (Figure 3). For the wild-type complex, in addition to the tunnel connecting the A-cluster and the C-cluster, exits were detected at the CODH/ACS interface and within the CODH dimer (Figure 3d). The tunnel with the largest bottleneck radius (1.03 Å) was the tunnel connecting the A-cluster A and the C-cluster. The smallest cross-section of CO measures 1.79 Å,[20] showing that conformational fluctuations are necessary for CO transport, and thus the relevance of each tunnel cannot be readily determined from a static crystal structure. However, the computed tunnel connecting the A-cluster and the C-cluster almost perfectly overlays with the Xenon binding sites found in the crystal structures of the homologous *M. thermoacetica* complex (Figure S10).[4,12] Furthermore, the F_o-F_c-map shows negative density in the tunnel region (Figure S10), indicating that the concentration of disordered water molecules in the tunnel is lower than in the bulk solvent. Disordered water molecules are generally assumed to surround protein crystal structures and are therefore taken into account in the bulk-solvent correction to calculate F_o-F_c-maps.[21] These features are in-

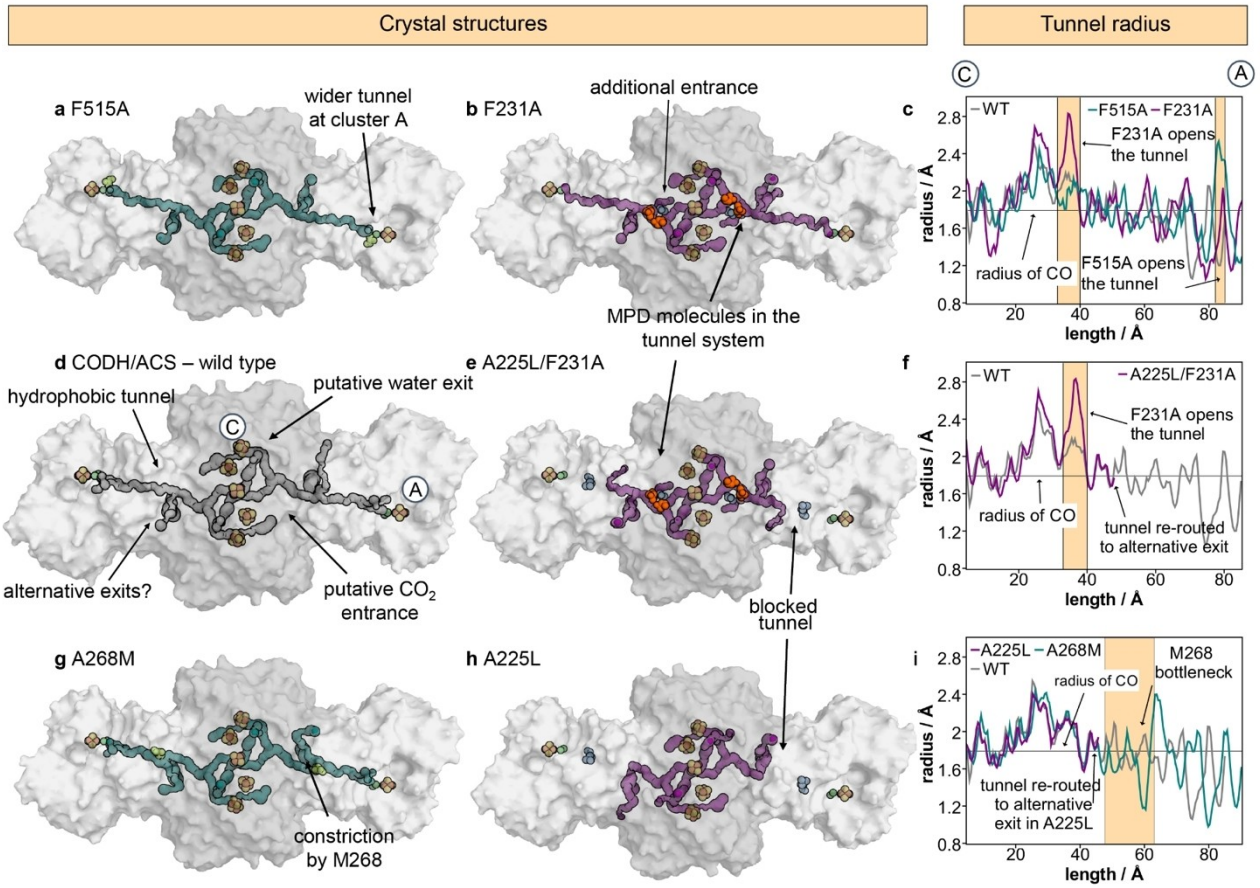

Figure 3. The tunnel system in the CODH/ACS complex variants. The structures are shown as surfaces colored light (ACS) and dark gray (CODH). The tunnel system is shown as a tube, the metal cluster (labeled in panel d), the MPD molecules (orange) and the respective exchanged amino acids (either bright green or light blue) are shown as spheres. Fe atoms are colored orange, S, yellow, Ni, green. Note that all structures possess a two-fold rotational symmetry and the rotation axis is located perpendicular to the paper plane at the D-cluster. Tunnels were computed using CAVER analyst 2.0[19] with a probe radius of 0.9 Å. a,b) Structure and tunnel system of the variants with an opened tunnel: F515A (a) and F231A (b). c) Comparison of the radius of the tunnel connecting the A-cluster and the C-cluster for the wild type (gray) and for the variants with an opened tunnel (same color as tunnel in the structures). The radius of CO is shown as black line. The position of important features and the locations of the A- and the C-clusters are indicated by labels. d,e) Structure and tunnel system of the wild type (d) and the A225L/F231A variant (e). f) Comparison of the radius of the tunnel connecting the A-cluster and the C-cluster for the wild type and for the A225L/F231A variant (labeling and coloring as panel c). g,h) Structure and tunnel system of the variants with a constricted tunnel: A268M (g) and A225L (h). i) Comparison of the radius of the tunnel connecting the A-cluster and the C-cluster for the wild type and for the variants with a constricted tunnel (labeling and coloring as panel c).

line with a highly hydrophobic tunnel between the A-cluster and the C-cluster.

Overall, the mutations altered the tunnel system as intended. The A268M and the A225L exchanges resulted in a narrowing of the tunnel, which in the case of A225L blocked the path from the C-cluster to the A-cluster (Figure 3a–c). The opening at the A-cluster due to the F515A exchange resulted in a widening of the tunnel system, whereas the F231A exchange opened a new tunnel branch connecting the tunnel to the solvent, as indicated by the presence of 2-methyl-2,4-pentanediol (MPD) molecules derived from the mother liquor in the tunnel system. And the A225L/F231A double mutant had the combined characteristics of both exchanges (Figure 3g–h).

Catalytic Activity of the Tunnel Variants

The catalytic activities in both partial reactions and in the coupled reaction (synthesis of acetyl-CoA from CO_2) were analyzed as a function of substrate concentration (Figure 4; Figures S11–S15). All tunnel variants were active catalysts for both CO_2 reduction and CO condensation. Furthermore, all variants were able to synthesize acetyl-CoA with CO_2 as the educt (Figure 5, Figure S16). Therefore, a continuous tunnel without branches leading to the solvent (as in the F231A exchange) is not essential for catalysis.

To compare the catalytic activities in the partial reactions, we normalized the values according to the degree of maturation of the C- and A-clusters, as determined by X-ray crystallography (Table S2, see Materials and Methods section for more information). In a previous study, we could

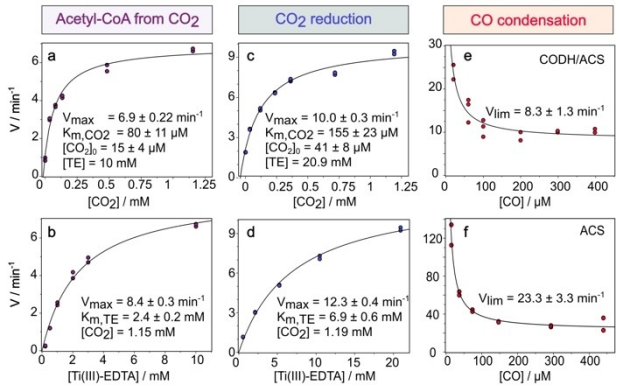

Figure 4. Catalytic activities of the wild type CODH-III/ACS complex and the isolated ACS subunit. All data were measured in 100 mM Mops/NaOH pH 7.2 supplemented with 3 mg/L carbonic anhydrase at 50 °C. For acetyl-CoA synthesis, the buffer was further supplemented with 200 µM CoA and 50 µM methylcobinamide. For the condensation reaction also 1 mM of Ti(III)-EDTA was present. The lines are fits with the equation shown in the materials and methods section. Relevant parameters and substrate concentrations are depicted in the plot. $[CO_2]_0$ denotes the intrinsic CO_2 concentration of the assay buffer. TE stands for Ti(III)-EDTA. a,b) Dependence of the rate of acetyl-CoA synthesis from CO_2 on either $[CO_2]$ (a) or [Ti(III)-EDTA] (b). c,d) Dependence of the CO_2 reduction rate on either $[CO_2]$ (c) or [Ti(III)-EDTA] (d). e,f) Dependence of the rate of the condensation of CO to acetyl-CoA on [CO] for the CODH/ACS complex (e) or the isolated ACS subunit (f).

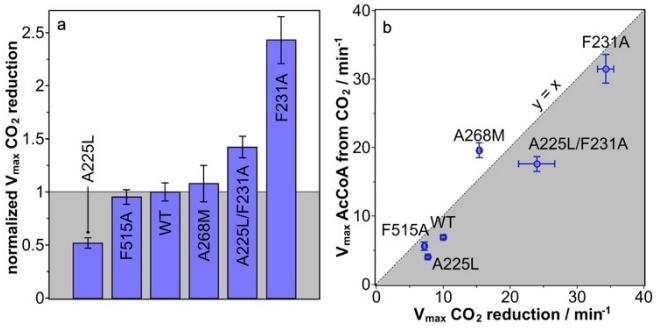

Figure 5. Normalized CO_2 reduction activities and correlation for the tunnel mutant. The activities were normalized on the wild type activity and the degree of cluster maturation. The activity of the wild type CODH-III/ACS with fully matured clusters equals 1. Error bars were calculated assuming a 5% error for the estimated maturation degree using the error of the fit for the kinetic parameters. a) CO_2 reduction activity of the variants. b) Correlation plot of the V_{max} in the acetyl-CoA synthesis from CO_2 and the V_{max} in CO_2 reduction. The shaded area in panel a indicates the wild-type activity and in panels b the region of the plot in which V_{max} in the acetyl-CoA synthesis from CO_2 is smaller than that of CO_2 reduction. The V-[S]-characteristics and the respective results for the K_m and K_i values for all variants can be found in the Supporting Information (Figures S11–S15).

show that the occupancy of the Ni atom of the C-cluster almost matches the relative CO oxidation activity compared to that of CODH-III/ACS directly isolated from *C. hydrogenoformans.*[6,9] The average occupancy of the Ni atom in the C-cluster was 36.5 ± 9.3 %. The average ratio of the Ni anomalous density at the proximal to that at the distal position is 0.38 ± 0.09, which can be translated into the percentage of Ni assuming 100 % Ni occupancy in the distal position and similar B-factors at both positions.

In CO_2 reduction, the variants with an additional tunnel entrance due to the F231A exchange were more active than the wild type. The A225L variant with a blocked tunnel had about 50 % of the wild-type activity. The A225L/F231A variant also showed a decrease in CO_2 reduction activity of about 50 % compared to the F231A variant, demonstrating that the tunnel blockage by L225 reproducibly decreases the CO_2 reduction activity. However, the F515A and the A268M variants had similar CO_2 reduction activities as the wild-type, indicating that the tunnel opening at the A-cluster and the slight constriction by M268 had little effect on CO_2 reduction. The CO_2 reduction activity of the CODH/ACS complex seems to be regulated by the bottlenecks of the tunnel system, as it can be increased or decreased by manipulating the tunnel.

In the CO condensation reaction, the A268M and F231A variants had significantly higher activity than the wild type (determined as V_{lim} at infinite CO concentration, see Supplement for more information). The A225L/F231A variant had significantly lower activity. Unfortunately, we cannot rationalize the different activities in CO condensation. However, they may be due to altered dynamics of the ACS subunit, which is essential for catalysis.[4,22] Nevertheless, all variants of the complex (Supporting Information) and the isolated ACS subunit (Figure 4f) showed the same response pattern to CO concentration: The rate of the condensation reaction decreased steadily with increasing CO concentration, reaching V_{lim} at infinite CO concentration. This indicates partial substrate inhibition of the enzyme by CO, where CO is bound with high affinity in an active state and with low affinity in a less active state, as has been previously described for the *M. thermoacetica* CODH/ACS complex.[23,24] These observations, together with the ITC data on the binding of CO to ACS, suggest that the methylated state is most likely the active, high-affinity state and the reduced state is the less active, low-affinity state that inhibits catalysis.

The characterization of the partial reaction also allows us to determine the rate-limiting step in the synthesis of acetyl-CoA from CO_2. The activity in the coupled reaction correlated more with the activity in the reduction of CO_2 (Figure 5) than with the activity in the CO condensation reaction. Furthermore, during acetyl-CoA synthesis, only low concentrations of the intermediate CO can build up transiently, as no CO leakage from the tunnel is observed.[10,11] The condensation reaction activity at low CO concentrations is much higher than the maximum CO_2 reduction rate for all variants. These two points support that in our experimental setup, CO_2 reduction was the rate-limiting step in the coupled reaction. We did not observe activation of CO_2 reduction when coupled to acetyl-CoA synthesis, as reported for the CODH/ACS complex of *M. thermoacetica.*[23]

Besides the effects on the activities, the tunnel manipulation also changed the K_m values for CO_2 and the electron donor Ti(III)-EDTA in both CO_2 reduction and acetyl-CoA

synthesis (Figure S17a). Of the two apparent $K_{m,TiEDTA}$ and $K_{m,CO2}$, only the latter is physiologically relevant. $K_{m,CO2}$ was similar in the coupled and in the partial reaction and differed in the CO_2 reduction by almost an order of magnitude between the variants (Figure S17b).

CO Transport in the Variants

Finally, we analyzed the gas transport for the tunnel variants (Figure 6). All substitutions decreased the efficiency of CO channeling into acetyl-CoA (Figure 6b). We quantified the tightness of CO transport by the percentage of CO-free hemoglobin in the steady-state phase of the reaction (Figure 6c).

While the F515A variant was as efficient as the wild-type, the A225L and A268M variants were much less efficient at channeling CO into acetyl-CoA and showed a biphasic appearance of Hb-CO in the reaction course. Variants carrying the F231A substitution could not prevent the loss of CO, as Hb-CO was already formed after the start of the reaction.

While it is readily understandable that an opening caused by the F231A exchange reduces the gas-tightness of the tunnel and thus impairs directed CO transport, the effects of the A225L and A268M exchanges cannot be explained by a simple gas-tight tube model. However, an overlay of the exchanged positions with the structure of the *M. thermoacetica* complex from xenon-pressurized crystals[4,12] may explain the findings. The overlay indicates that the A225L and A268M exchanges may block access to isolated hydrophobic binding sites for Xe in the tunnel (Figure S10, inset).

Thus, the tunnel might be seen as a bucket brigade of CO binding sites rather than as a simple tube connecting the C-cluster and the A-cluster. The A225L and A268M exchanges, or solvent molecules entering the tunnel through the F231A hole, might block access to some of the binding sites of this bucket brigade and thus affect the overall efficiency of transport. The biphasic appearance of Hb-CO for the A225L and A268M variant might be due to slightly lowered affinity of the hydrophobic binding sites in the tunnel: At reaction start, CO preferably binds to hemoglobin and upon partial saturation of hemoglobin preferably in the tunnel.

Furthermore, this experiment provides a clue to the observed coupled kinetics of the monofunctional enzymes where we were wondering, what caused the preferential channeling of CO into acetyl-CoA: Fast binding of CO at the A-cluster or pre-concentration and sequestration of CO in the tunnel? If CO binding to the A-cluster would be much faster than to hemoglobin, we wouldn't expect the A225L, A268M and F231A variants to perform worse than the wild-type in CO-channeling. In these variants the CO binding rate to the A-cluster is probably not affected by these mutations far from the A-cluster. Thus, if these mutations would just simply create cracks in the tube, CO could be still channeled to the A-cluster. This is not the case. Thus, the rate of binding to the A-cluster is not the reason for the channeling of CO and it might be rather the formation of a separate CO pool through hydrophobic binding in the tunnel, which is sequestered from bulk water and thus from hemoglobin.

Overall, as the A268M, A225L and the F231A exchanges led to a decreased channeling efficiency, while splitting the complex did not, we conclude that the blockade of hydrophobic binding pockets in the tunnel by bulky amino acids (A268M, A225L) or by the intrusion of solvent molecules (F231A) caused a lower channeling efficiency.

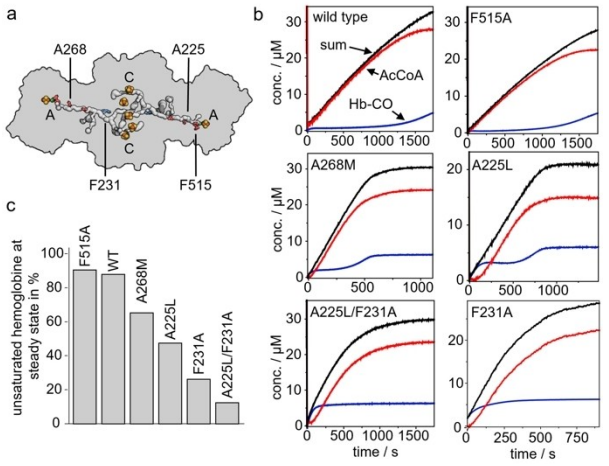

Figure 6. CO transport during catalysis for the CODH/ACS complex variants. The competition experiment was always carried out in 0.1 M Mops/NaOH pH 7.2 supplemented with 0.3 mg/L carbonic anhydrase, 200 µM CoA, 50 µM methylcobinamide, 10 mM Ti(III)-EDTA, and 1.2 mM CO_2, if not otherwise stated. a) Structure and tunnel system of the CODH/ACS complex (PDB 7ZKJ). The shape of the complex is shown in gray. The exchanged residues are shown as sticks and labeled at one site of the two-fold symmetric complex. The label C and A indicate the position of the C-cluster and the A-cluster, respectively. The presentation is otherwise the same as in Figure 3. b) Competition experiment traces for the tunnel variants. [Hb-CO] blue, [AcCoA] red, sum black. Deviating substrate and enzyme concentrations were 0.22 µM (WT), 0.55 µM (F515A), 0.5 µM (A268M), 0.55 µM (A225L), and 2.32 mM CO_2, 5.1 mM Ti(III)-EDTA (F231A) variant (0.38 µM enzyme) and 0.46 µM (A225L/F231A) and ca. 7 µM Hb for all variants. c) Tightness of the tunnel system in the variants determined as the percentage of free hemoglobin when the acetyl-CoA production reached the steady state.

Conclusion

Both *Moorella* and *Carboxydothermus* CODH/ACS complexes are stable protein assemblies containing a tight tunnel for CO diffusion between the two active sites. It is likely that both traits evolved during the transition from mono- to bifunctional CODHs. These features seem to be irrelevant for catalytic efficiency, since the coupled reaction between monofunctional CODH and ACS works efficiently, and manipulations of the tunnel by opening it can even increase the overall turnover. So, why have these stable complexes with narrow tunnels evolved?

By manipulating the tunnel, we showed that the flux through the tunnel controls the output of CO from the CODH subunit. Furthermore, the coupled reaction is probably rate-limited by the reduction of CO_2 and not by the condensation of CO at the A-cluster, which could occur at much higher rates in our experimental setup. All tunnel variants, even those with a blocked tunnel, catalyze the coupled reaction - the synthesis of acetyl-CoA from CO_2. However, the efficiency of channeling CO into acetyl-CoA was impaired. While there is essentially no CO leakage from the tunnel during catalysis with the wild-type CODH/ACS, significant leakage was found for the variants with a constricted tunnel (A268M, A225L) and for the variants whose tunnel was opened by the F231A exchange at the CODH/ACS-interface. The F515A exchange near the A-cluster left the CO transport almost unaffected.

While an increased leakiness due to an opening readily explains our observed kinetics, the effect of the constrictions seems to go beyond a simple hindrance of CO diffusion within the tunnel. Rather, the constrictions reduce CO channeling efficiency by blocking the access to hydrophobic CO binding sites in the tunnel. This mode of CO transport is also supported by the surprising observation that CO is efficiently channeled into acetyl-CoA using the isolated ACS subunit and the monofunctional CODH-II. Apparently, an intact continuous tunnel between the C-cluster and the A-cluster is not needed to achieve efficient channeling of CO into acetyl-CoA, but rather bucket-brigade-like transport of CO between internal hydrophobic binding sites inside the ACS enzyme (Figure 7). Thus, the evolution of a stable complex between CODH and ACS may have simply extended and stabilized this transport system.

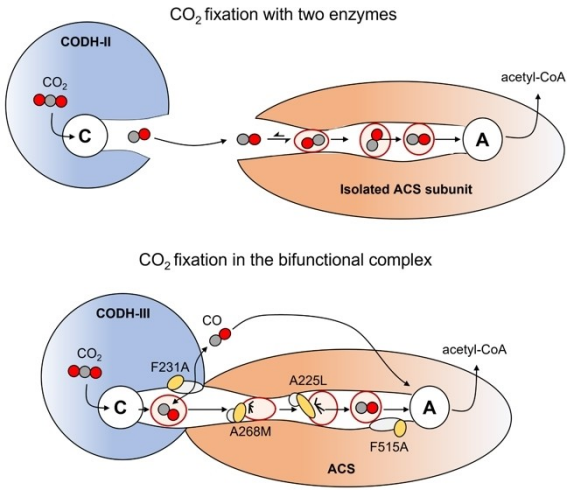

Figure 7. The role of the tunnel in catalysis. The tunnel is shown as a stylized tube connecting the C- and A-cluster. The exchanged residues are drawn schematically as white ellipsoids and the introduced residues as yellow ellipsoids. CO and CO_2 are shown as spheres and the hydrophobic binding sites as red circles. The introduction of bulky residues might decrease the accessibility of the binding sites in the tunnel, explaining why the constricting amino acid exchanges A225L and A268M led to an increased leakiness of the tunnel. The exchanges F231A and F515A open the tunnel. However, only the F231A exchange led to a considerable leakage of CO, which could then reach the A-cluster through the solvent. Furthermore, even with the isolated ACS subunit, CO in solution is probably captured by the hydrophobic binding sites, ensuring efficient channeling of CO into acetyl-CoA.

Supporting Information

The authors have cited additional references within the Supporting Information.[25–48]

Acknowledgements

We acknowledge access to beamlines of the BESSY II storage ring (Berlin) through the Joint Berlin MX-Laboratory sponsored by Helmholtz Zentrum Berlin für Materialien und Energie, Freie Universität Berlin, Humboldt-Universität zu Berlin, Max-Delbrück-Centrum, and the Leibniz-Institut für Molekulare Pharmakologie. This work was funded by the Deutsche Forschungsgemeinschaft (DFG, German Research Foundation) under Germany's Excellence Strategy—EXC 2008-390540038-UniSysCat. The authors acknowledge the funding agency DFG for support of the project through grant DO785/6-2. Open Access funding enabled and organized by Projekt DEAL.

Conflict of Interest

The authors declare no conflict of interest.

Data Availability Statement

Coordinates and structure factor amplitudes are available in the Protein Data Bank (https://www.ebi.ac.uk/pdbe/) under accession numbers 8CJB, 8CMW, 8CJA and 8CJC.

Keywords: Carbon monoxide dehydrogenase · Catalytic coupling · Nickel · CO_2 · Substrate tunnel

[1] S. W. Ragsdale, *Ann. N. Y. Acad. Sci.* **2008**, *1125*, 129–136.
[2] G. Fuchs, *Annu. Rev. Microbiol.* **2011**, *65*, 631–658.
[3] T. I. Doukov, T. M. Iverson, J. Seravalli, S. W. Ragsdale, C. L. Drennan, *Science* **2002**, *298*, 567–572.
[4] C. Darnault, A. Volbeda, E. J. Kim, P. Legrand, X. Vernède, P. A. Lindahl, J. C. Fontecilla-Camps, *Nat. Struct. Mol. Biol.* **2003**, *10*, 271–279.
[5] O. N. Lemaire, T. Wagner, *Biochim. Biophys. Acta Bioenerg.* **2020**, *1862*, 148330.
[6] J. Ruickoldt, Y. Basak, L. Domnik, J.-H. Jeoung, H. Dobbek, *ACS Catal.* **2022**, *12*, 13131–13142.
[7] M. Can, F. A. Armstrong, S. W. Ragsdale, **2014**, *114*, 4149–4174.
[8] S. Gencic, D. A. Grahame, *J. Biol. Chem.* **2003**, *278*, 6101–6110.

[9] V. Svetlitchnyi, H. Dobbek, W. Meyer-Klaucke, T. Meins, B. Thiele, P. Römer, R. Huber, O. Meyer, *Proc. Natl. Acad. Sci. USA* **2004**, *101*, 446–451.
[10] E. L. Maynard, P. A. Lindahl, *J. Am. Chem. Soc.* **1999**, *121*, 9221–9222.
[11] J. Seravalli, S. W. Ragsdale, *Biochemistry* **2000**, *39*, 1274–1277.
[12] T. I. Doukov, L. C. Blasiak, J. Seravalli, S. W. Ragsdale, C. L. Drennan, *Biochemistry* **2008**, *47*, 3474–3483.
[13] X. Tan, H.-K. Loke, S. Fitch, P. A. Lindahl, *J. Am. Chem. Soc.* **2005**, *127*, 5833–5839.
[14] X. Tan, A. Volbeda, J. C. Fontecilla-Camps, P. A. Lindahl, *J. Biol. Inorg. CheJ. Biol. Inorg. Chem.m.m.* **2006**, *11*, 371–378.
[15] X. Tan, P. A. Lindahl, *J.Biol. Inorg. Chem.* **2008**, *13*, 771–778.
[16] P.-h. Wang, M. Bruschi, L. De Gioia, J. Blumberger, *Journal of the American Chemical Society* **2013**, *135*, 9493–9502.
[17] M. Can, M. J. Abernathy, S. Wiley, C. Griffith, C. D. James, J. Xiong, Y. Guo, B. M. Hoffman, S. W. Ragsdale, R. Sarangi, *J. Am. Chem. Soc.* **2023**, *145*, 13696–13708.
[18] J. Bao, S. M. Krylova, L. T. Cherney, J. C. Y. LeBlanc, P. Pribil, P. E. Johnson, D. J. Wilson, S. N. Krylov, *Anal. Chem.* **2014**, *86*, 10016–10020.
[19] A. Jurcik, D. Bednar, J. Byska, S. M. Marques, K. Furmanova, L. Daniel, P. Kokkonen, J. Brezovsky, O. Strnad, J. Stourac, A. Pavelka, M. Manak, J. Damborsky, B. Kozlikova, *Bioinformatics* **2018**, *34*, 3586–3588.
[20] R. Banerjee, J. D. Lipscomb, *Acc. Chem. Res.* **2021**, *54*, 2185–2195.
[21] P. V. Afonine, R. W. Grosse-Kunstleve, P. D. Adams, A. Urzhumtsev, *Acta Crystallogr. Sect. D* **2013**, *69*, 625–634.
[22] S. E. Cohen, E. J. Brignole, E. C. Wittenborn, M. Can, S. Thompson, S. W. Ragsdale, C. L. Drennan, *Structure* **2020**.
[23] E. L. Maynard, P. A. Lindahl, *Biochemistry* **2001**, *40*, 13262–13267.
[24] A. Biester, S. Dementin, C. L. Drennan, *J. Inorg. Biochem.* **2022**, *230*, 111774.
[25] J.-H. Jeoung, H. Dobbek, *Science* **2007**, *318*, 1461–1464.
[26] U. Mueller, R. Förster, M. Hellmig, F. U. Huschmann, A. Kastner, P. Malecki, S. Pühringer, M. Röwer, K. Sparta, M. Steffien, M. Ühlein, P. Wilk, M. S. Weiss, *Eur. Phys. J. Plus* **2015**, *130*.
[27] K. M. Sparta, M. Krug, U. Heinemann, U. Mueller, M. S. Weiss, *J. Appl. Crystallogr.* **2016**, *49*, 1085–1092.
[28] W. Kabsch, *Acta Crystallogr. Sect. D* **2010**, *66*, 125–132.
[29] P. Emsley, B. Lohkamp, W. G. Scott, K. Cowtan, *Acta Crystallogr. Sect. D* **2010**, *66*, 486–501.
[30] D. Liebschner, P. V. Afonine, M. L. Baker, G. Bunkóczi, V. B. Chen, T. I. Croll, B. Hintze, L.-W. Hung, S. Jain, A. J. McCoy, N. W. Moriarty, R. D. Oeffner, B. K. Poon, M. G. Prisant, R. J. Read, J. S. Richardson, D. C. Richardson, M. D. Sammito, O. V. Sobolev, D. H. Stockwell, T. C. Terwilliger, A. G. Urzhumtsev, L. L. Videau, C. J. Williams, P. D. Adams, *Acta Crystallogr. Sect. D* **2019**, *75*, 861–877.
[31] S. Keller, C. Vargas, H. Zhao, G. Piszczek, C. A. Brautigam, P. Schuck, *Anal. Chem.* **2012**, *84*, 5066–5073.
[32] C. A. Brautigam, H. Zhao, C. Vargas, S. Keller, P. Schuck, *Nat. Protoc.* **2016**, *11*, 882–894.
[33] H. Zhao, G. Piszczek, P. Schuck, *Methods* **2015**, *76*, 137–148.
[34] W. D. Robertson, A. M. Bovell, K. Warncke, *JBIC J. Biol. Inorg. Chem.* **2013**, *18*, 701–713.
[35] M. Yoshino, K. Murakami, *Springerplus* **2015**, *4*.
[36] A. Mitchell, H.-Y. Chang, L. Daugherty, M. Fraser, S. Hunter, R. Lopez, C. McAnulla, C. McMenamin, G. Nuka, S. Pesseat, A. Sangrador-Vegas, M. Scheremetjew, C. Rato, S.-Y. Yong, A. Bateman, M. Punta, T. K. Attwood, C. J. A. Sigrist, N. Redaschi, C. Rivoire, I. Xenarios, D. Kahn, D. Guyot, P. Bork, I. Letunic, J. Gough, M. Oates, D. Haft, H. Huang, D. A. Natale, C. H. Wu, C. Orengo, I. Sillitoe, H. Mi, P. D. Thomas, R. D. Finn, *Nucleic Acids Res.* **2015**, *43*, D213–21.
[37] K. Katoh, D. M. Standley, *Mol. Biol. Evol.* **2013**, *30*, 772–780.
[38] K. Katoh, *Nucleic Acids Res.* **2002**, *30*, 3059–3066.
[39] B. Q. Minh, H. A. Schmidt, O. Chernomor, D. Schrempf, M. D. Woodhams, A. von Haeseler, R. Lanfear, *Mol. Biol. Evol.* **2020**, *37*, 1530–1534.
[40] S. Kalyaanamoorthy, B. Q. Minh, T. K. F. Wong, A. von Haeseler, L. S. Jermiin, *Nat. Methods* **2017**, *14*, 587–589.
[41] S. Q. Le, O. Gascuel, *Mol. Biol. Evol.* **2008**, *25*, 1307–1320.
[42] A. M. Kozlov, D. Darriba, T. Flouri, B. Morel, A. Stamatakis, *Bioinformatics* **2019**, *35*, 4453–4455.
[43] F. D. K. Tria, G. Landan, T. Dagan, *Nat. Ecol. Evol.* **2017**, *1*, 193.
[44] S. A. Ishikawa, A. Zhukova, W. Iwasaki, O. Gascuel, T. Pupko, *Mol. Biol. Evol.* **2019**, *36*, 2069–2085.
[45] K. N. Orlandi, S. R. Phillips, Z. R. Sailer, J. L. Harman, M. J. Harms, *Protein Sci.* **2023**, *32*, e4551.
[46] C. K. Saha, R. Sanches Pires, H. Brolin, M. Delannoy, G. C. Atkinson, *Bioinformatics* **2021**, *37*, 1312–1314.
[47] I. Letunic, P. Bork, *Nucleic Acids Res.* **2021**, *49*, W293–W296.
[48] P. Kuzmic, *Methods Enzymol.* **2009**, *467*, 247–280.

Manuscript received: March 14, 2024
Accepted manuscript online: May 14, 2024
Version of record online: June 25, 2024